The snapping shrimp dactyl plunger: a thermomechanical damage tolerant sandwich composite

The snapping shrimp dactyl plunger: a thermomechanical damage-tolerant sandwich composite

Parvez Alam[1]*, Immanuel Sanka[2, 3], Lilja Piuli Alam[4], Saka Wijaya[5], Erly Sintya[1, 3, 6], Niken Satuti Nur Handayani[7], Adolfo Rivero-Müller[8,9]

[1] School of Engineering, Institute for Materials and Processes, University of Edinburgh, Edinburgh, UK
[2] Biology Education Centre, Uppsala University, Uppsala, Sweden
[3] KSK-Biogama (Marine Biology Study Group), Faculty of Biology, Universitas Gadjah Mada, Yogyakarta, Indonesia
[4] International Baccalaureate School, Turku, Finland
[5] Department of Tropical Biology, Faculty of Biology, Universitas Gadjah Mada, Yogyakarta, Indonesia
[6] Department of Imaging Sciences & Biomedical Engineering Research Division, Kings College, London, UK
[7] Laboratory of Genetics and Breeding, Faculty of Biology, Universitas Gadjah Mada, Yogyakarta, Indonesia
[8] Turku Centre for Biotechnology, University of Turku and Åbo Akademi University, Turku, Finland
[9] Department of Biochemistry and Molecular Biology, Medical University of Lublin, Lublin, Poland

***Corresponding author.**

Email addresses: parvez.alam@ed.ac.uk, parvez.alam@abo.fi

Highlights

- Snapping shrimps were found to have highly pressurised dactyl plungers with sandwich composite cross-sections.
- The composite is structured with hard outer layers and a ca. 50% porous, chitin middle layer.
- Finite element models reveal that the middle layer is able to insulate against heat and absorb mechanical energy.
- Plungers are subjected to high pressures/heat and the dactyl plunger exhibits a design with thermomechanical damage tolerance.

Abstract

The dactyl plunger of *Alpheus* sp. was found to be a layered composite, with mineral-rich outer and inner layers and a chitin-rich middle layer of high porosity. The chitin-rich middle layer is itself composed of several porous chitin laminae. Modelling heat conduction through the plunger cross-section revealed that the chitin-rich layer is able to insulate heat and retard its progress through the material. Heat accumulates in the plunger after a series of successive snaps and as such, its thermally resistant design can be considered most useful under the conditions of successive snapping. The plunger has a concurrent mechanical damage-tolerant design with biogenic mineral layers, viscous (chitin–mineral) interfaces, energydissipating porous chitin, and sidewalls composed of ordered, layered aragonite. The snapping shrimp plunger has a design that may protect it and internal soft tissues from thermomechanical damage during plunger–socket compression prior to cavitation bubble release.

Keywords: Snapping shrimp; Dactyl plunger; Sandwich composite; Biomimetics; Bio-architecture

1. Introduction

Snapping shrimps comprise a specialised family (Alpheidea) of arthropods with asymmetrical chelae (Fig. 1), the larger of which produces a highly audible and explosive snapping sound. Though earlier reports hypothesised that the explosive sound is a result of physical impact between the finger and thumb of the chela (Johnson et al., 1947), it is now understood that the sound is due to the collapse of a cavitation bubble outside the chela. This bubble is formed by compression of air between a plunger and socket within the chela (Fig. 2) and exits the chela at a velocity of 7–32 m/s (Herberholz and Schmitz, 1999; Versluis et al., 2000), collapsing a few millimetres from the tip of the chela (Versluis et al., 2000) and releasing an explosive acoustic sound of approximately 190 dB (Fergusson and Cleary, 2001). The immediate external pressure drop, after the bubble exits, is in the order of ca. 0.1–0.3 MPa (Versluis et al., 2000; Kim et al., 2010; Hess et al., 2013). The sound intensity of the cavitation bubble collapse is close to that of the mono-pulsed sperm whale click, which has been recorded at ca. 236 dB (Mohl et al., 2003), making the snapping shrimp one of the loudest extant marine animals. Sonoluminescence is produced alongside extreme heat as the cavitation bubble collapses. The temperature approaches the surface temperature of the sun (Downer, 2002) at around 5000 K, presumably due to high compression in the final stages of the cavitation bubble collapse (McNamara et al., 1999). Acoustic pressure pulses that arise through cavitation bubble collapse are typically in the order of 700 kPa (Lohse et al., 2001). Several factors will affect the bubble sizes and velocities. Amongst the more prominently mentioned in the literature are: chela shape (Kim et al., 2010), the rate and style of snapping closure (Ritzmann, 1974; Mellon and Stephens, 1979; Mellon, 1981), and the gender of the shrimp – males of similar size to females generate bubbles with higher velocity (Herberholz and Schmitz, 1999) whilst also possessing stouter chelae than similar-sized females.

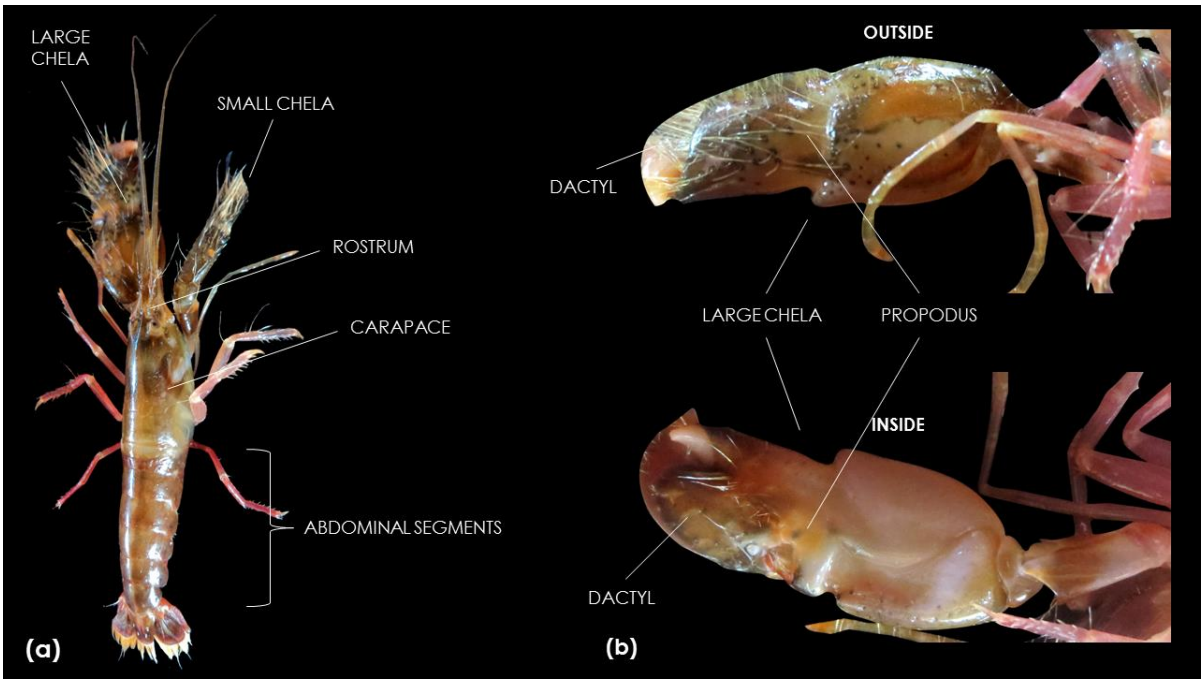

Fig. 1. (a) Snapping shrimp external morphology from the dorsal view; (b) enlarged view of the large chela as observed from both the inside (ventral) and outside (dorsal) view.

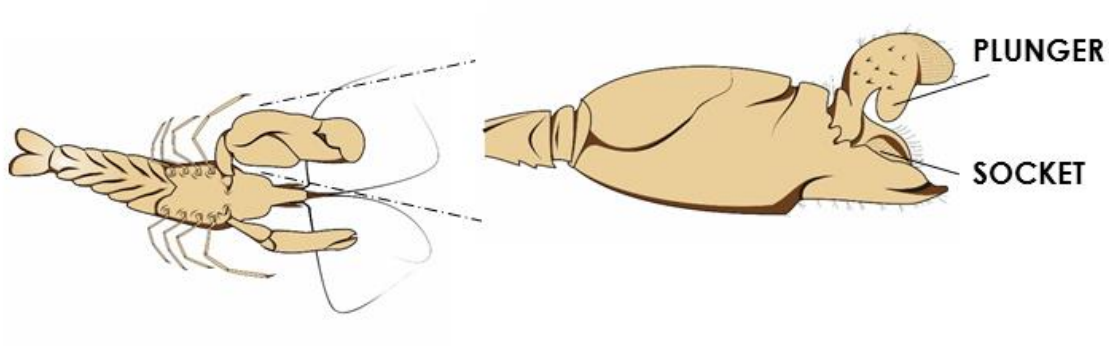

Fig. 2. Schematic drawing showing the plunger–socket system of the snapping shrimp.

While there are several researchers who have considered the acoustics of snapping (Everest et al., 1948; Au and Banks, 1997; Legg et al., 2007) and the physics associated with cavitation bubble collapse (Versluis et al., 2001; Chitre et al., 2003), neither the compressive pressures nor the heat energy *within* the socket during plunger compaction have been reported in the literature. To date, very little has been reported on the snapping shrimp dactyl plunger. Johnson et al. (1947) noted high levels of calcification at the tips of the chela. Beyond this, we find no reports on either the material or the architectural characterisation of the enlarged chela of the snapping shrimp. Yet, plunger–socket compressive pressures, heat generation due to the compression, and the shock waves resulting from 'snapping' are all potential sources of damage to the materials of the chela, most prominently in the area of the plunger–socket system. For the plunger–socket system to survive repeated pressurisation and the resultant temperatures and shock waves, it logically requires a material design that can withstand coupled thermomechanical energies.

Here, we hypothesise that special architectures imparting damage tolerance will exist in the snapping shrimp dactyl plunger. In particular, we posit that these architectures will exhibit a design able to withstand high heat and mechanical forces. Our objectives for this paper are to characterise the microarchitecture of the plunger both physically and chemically. We consider the plunger to be the most logical startingpoint since it is directly involved with compression and cavitation bubble creation, and is thus exposed to both mechanical and thermal energies during the process of 'snapping'.

2. Materials and methods

2.1. Bioprospecting and capture of snapping shrimps

Nocturnally active snapping shrimp were collected overnight at Pantai Drini, Gunug Kidul, Java, Indonesia (8.1385° S, 110.5775° E) during November 2014 and a second time during January 2016. Shrimps were killed by indirect icing, which was subsequently followed by freezing, by which means the shrimps were also preserved. The treatment and killing of shrimps followed guidelines from both the European Union Financial Instrument for Fisheries Guidance (FIFG) and the NIH Guide for Care and Use of Laboratory Animals. Ten shrimps were captured in total over the two separate expeditions.

2.2. Genetic and morphological identification of the shrimps

Two loci of the pistol shrimp mitochondrial genome were amplified using universal COI and 16S primers according to Folmer et al. (1994) and Hultgren and Stachowicz (2008), respectively (Table 1). DNA was isolated from the limb tissues of the shrimp and extracted using Chelex 10%. The extraction was conducted at a temperature of 95 °C for 30–45 min, and followed by sodium acetate and alcohol precipitation. High-fidelity polymerase (KOD Xtreme polymerase; Millipore) was used for DNA amplification. The polymerase chain reaction (PCR) cycle and temperature were consecutively set at 30 s pre-denaturation (96 °C); 40 cycles of 30 s denaturation (94 °C), 30 s annealing (49 °C for COI and 50–58.5 °C for 16S), and 60 s elongation (68 °C); it ended with 90 s final extension (72 °C). The results produced included sequences of 680 bp (COI) and 420 bp (16S), which were sequenced using the Turku Centre for Biotechnology (Finland) sequencing service. The sequences were BLASTed into the GenBank database in order to find their relevant adjacent homology. MUSCLE alignment was needed to construct a phylogenetic tree using a neighbour-joining statistical method in MEGA6 (Saitou and Nei, 1987; Edgar, 2004; Tamura et al., 2004, 2013).

Table 1. Primers for DNA barcoding.

16S (Hultgren and Stachowicz, 2008)	Forward:	(5'-TATT TTGA CCGT GCAA AGGT AG-3')
	Reverse:	(5'-ATTT AAAG GTCG AACA GACC CT-3')
COI (universal) (Folmer et al., 1994)	LCO1490:	(5'- GGTCAACAAATCATAAAGATATTGG-3')
	HCO2198:	(5'- TAAACTTCAGGGTGACCAAAAAATCA-3')

Morphological identification was conducted using descriptions available in Holthuis (1980), Kim and Abele (1988), and Anker et al. (2006).

2.3. Chemical characterisation of the plunger

Energy dispersive X-ray spectroscopy (EDS) was used to determine the elemental composition of the plunger cross-section. Fourier transform infra-red spectroscopy (FTIR) was used in ATR mode to identify prominent chemical groups as well as the polymorphic forms of metal carbonates present in the plunger.

2.4. Optical characterisation of the plunger

A plunger was immersed in liquid nitrogen for 3 min to embrittle the material. As soon as the plunger was removed from the liquid nitrogen, it was fractured through its meridional axis to reveal its inner cross-section. The fracture was instigated using a thin single-edged blade which initiated fracture through a short, sharp impact to one end of the plunger. This procedure was repeated on three separate plungers to discern whether similar architectures were visible in different specimens. Images of the plunger were obtained by scanning electron microscopy (SEM). Image analysis software Image-J was subsequently used to approximate the dimensions and area fractions of the plunger and its components from the SEM images. The porosity was thus computed using the image analysis software.

2.5. Heat transfer and continuum mechanics modelling

To determine thermal transience through the plunger we developed a finite element model where the inner, middle and outer layers of the plunger were constructed using separate geometries connected only at their interfaces (Fig. 3. The dimensions for each layer were determined using image analysis measurements from SEM micrographs (cf. Fig. 4) and we simulated a symmetry model using only half the cross-section. The fundamental convection–conduction model is shown in Equation 1:

$$\rho C_p \frac{\partial T}{\partial t} + \nabla \cdot (-k\nabla T) = Q - \rho C_p \mathbf{u} \cdot \nabla T \qquad (1)$$

where ρ = density, C_p = specific heat capacity, T = temperature, k = thermal conductivity, t = time, $\mathbf{u}$ = velocity vector, Q = heat sources.

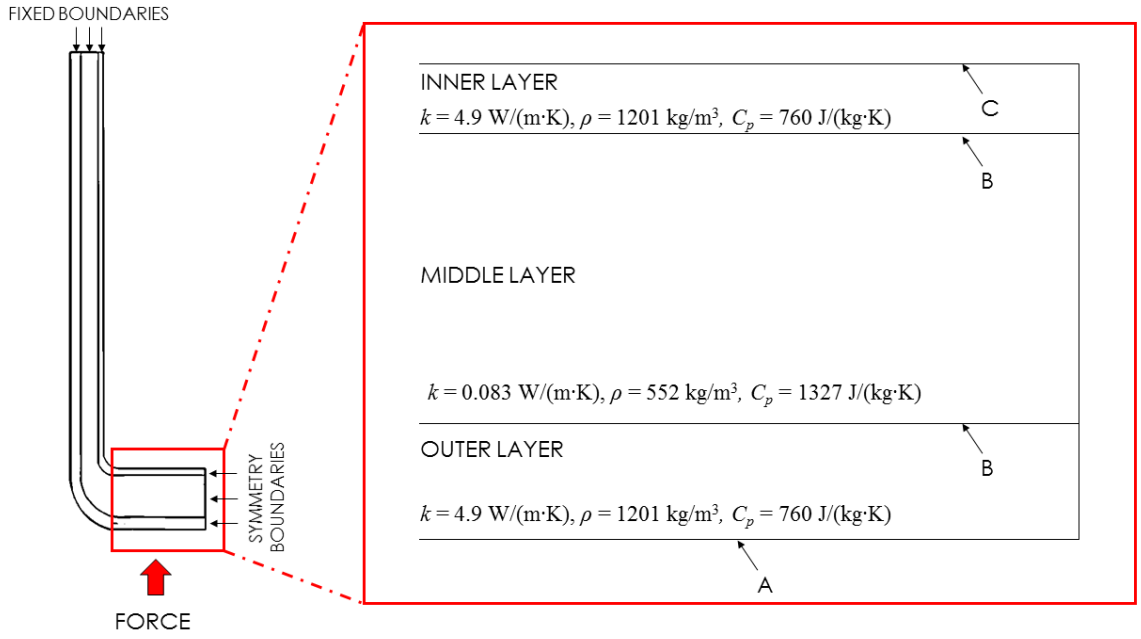

Fig. 3. Modelled thermal properties through the plunger cross-section and boundary conditions A, B, and C.

Boundary conditions A, B, and C (see Fig. 3) are represented by Equations 2, 3, and 4, respectively, where **q** is the vector for conductive flux and **n** is the normal vector for convective heat flux. Though the temperatures generated inside the snapping shrimp plunger–socket system are still unknown, due to the high speed and pressure that build up inside this system, the temperature is presumably high. The temperature developing inside the snapping shrimp plunger was calculated according to Equation 5, where T_f is the final temperature, T_i is the starting temperature, P_f is the final pressure and P_i is the initial pressure. We make the assumption that the pressure generated as the bubble is released from the plunger–socket system is comparable to the pressure within the system just prior to 'shooting'. Bernoulli's theorem can be used to estimate the dynamic pressure drop as the bubble exits with speed. This pressure has been reported to be within a magnitude of ca. 0.1–0.3 MPa (Versluis et al., 2000; Kim et al., 2010; Hess et al., 2013). Assuming the starting

temperature to be 300 K and the starting pressure to be a hydrostatic pressure at approximately 10 cm below water (9800 Pa), we find the final expected temperature to be ca. 3000–9000 Kelvin, which is similar to the actual temperature of cavitation bubble collapse (McNamara et al., 1999). Here, a mid-range temperature, T_0, of ca. 6000 K was applied to the boundary.

$$T = T_0 \qquad (2)$$

$$\mathbf{q_i} = -k_i \nabla T_i + \rho_i C_{pi} T_i \mathbf{u_i} \qquad (3)$$

$$\mathbf{n} \cdot (-k \nabla T) = 0 \qquad (4)$$

$$T_f = \frac{P_f}{P_i} T_i \qquad (5)$$

We ran two conduction models to develop an understanding of (a) heat transfer through the plunger system as a function of plunger hold time (Stein, 1975) and (b) heat transfer through the plunger system as heat is applied in succession (i.e. one shot after another). In the first model, we applied heat at the base of the plunger for 1, 2, 3, 4 and 5 ms. In the second model, we used a lower initial heat (T_0 = 3000 K), ran the simulation for 1 ms, and performed 3 'shots' in succession based on Levinton et al. (1995).

Numerical values of C_p, k and ρ are provided for each layer in Fig. 3. For the outermost and innermost layers, the values of k were taken from Clauser and Huenges (1995) and were set at 4.9 $Wm^{-1}K^{-1}$ for carbonates containing both magnesium and calcium. In the article by Clauser and Huenges (1995), pure calcites are reported as being in a similar range (ca. 4.2–5 $Wm^{-1}K^{-1}$) and as such, the substitution of magnesium within the calcite does not appear to have any manifest influence on its thermal conductivity. Since the middle layer was essentially a porous chitin–air system, we determined the effective thermal conductivity, K, using a Maxwell-Eucken formulation, Equation 6 (Buonanno and Carotenuto, 2000; Rocha and Cruz, 2001; Wang et al., 2006). Here k_1 represents the thermal conductivity of chitin and is given a value of 0.15 $Wm^{-1}K^{-1}$ (Muzzarelli, 1977; Warren, 2010), and k_2 the thermal conductivity of air, which is 0.0265 $Wm^{-1}K^{-1}$ (Boomsma and Poulikakos, 2001), while a_1 and a_2 represent the relative area fractions of chitin and air, respectively. The area fractions were averaged from image analysis computations (ImageJ) on three separate SEM images taken at a ×3K magnification. The specific heat capacity of chitin was inferred from Uryash et al. (2012) and the density from Muzzarelli (1977). For the inner and outer layers, the value of specific heat was inferred from Jacobs et al. (1981) and the density of biogenic calcite was taken from Vogel (2003). For the middle layer of the plunger, the values for C_p and ρ were averaged with air using a simple parallel series model.

$$K = \frac{k_1 a_1 + k_2 a_2 \frac{3k_1}{2k_1 + k_2}}{a_1 + a_2 \frac{3k_1}{2k_1 + k_2}} \qquad (6)$$

We used the same geometrical model to also simulate stress transfer through the plunger with respect to force applied to the bottom of the plunger. We concurrently used a plane stress formulation (Equations 7 and 8). In these equations, E is the elastic modulus, σ is

stress, ε is strain, and ν is Poisson's ratio. The orthogonal Cartesian axes are represented by the subscripts 1-3. A force of 60 N was applied to the bottom of the plunger system, which is a value lying within the range of measured closing forces (Elner and Campbell, 1981; Block and Rebach, 1998). The values of E for the outer and inner layers of the mineral-rich regions of the plunger were set at 60 GPa, while E for the porous chitin-rich region was given a value of 2.5 GPa, which is half the modulus of the helicoidal chitin structure in Weaver et al. (2012), but accounting for approximately 50% porosity using a simple law of mixtures.

$$\sigma_{31} = \sigma_{13} = \sigma_{32} = \sigma_{23} = \sigma_{33} = 0 \qquad (7)$$

$$\begin{pmatrix} \sigma_{11} \\ \sigma_{22} \\ \sigma_{12} \end{pmatrix} = \frac{E}{1-\vartheta^2} \begin{bmatrix} 1 & \vartheta & 0 \\ \vartheta & 1 & 0 \\ 0 & 0 & \frac{1-\vartheta}{2} \end{bmatrix} \cdot \begin{pmatrix} \varepsilon_{11} \\ \varepsilon_{22} \\ 2\varepsilon_{12} \end{pmatrix} \qquad (8)$$

3. Results

3.1. Identification of species

Morphological identification was supplemented with genetic barcoding (details are provided in the supplementary online Appendix) and we deduced the shrimp to be an *Alpheus* species.

3.2. Optical characterisation of the plunger cross-section

Foremost, we noticed that the fracture surface of a cleaved representative plunger (Fig. 4a) is a layered structure and has the appearance of a sandwich composite consisting of inner, middle and outer layers, denoted as [i], [ii] and [iii], respectively, in Fig. 4b. Magnifications of the middle layer (Fig. 4c and d) revealed a systematic array of interlocking "pine-tree"-like structures, which are, in turn, arranged into separated, yet conjoined laminae. These laminae are widest closest to the outermost layer, progressively becoming narrower as they approach the innermost layer (Fig. 4c). The narrowest of these pine-tree laminae are approximately one tenth of the widest in width, which might be an attribute related to growth and the speed at which cellular material is released. In Fig. 5, we note that the pine-tree-like structures extend to the top of the plunger. Importantly in Fig. 5b, we observe that, at the top of the plunger, the outermost layer is in fact made up of two layers in itself, [iii-A] and [iii-B], something which was not observed at the bottom of the plunger (cf. Fig. 4b). This characteristic was mirrored in each of the three snapping shrimp plungers imaged. In Fig. 5b [iii-B], the layer exhibits an organised plate-like structure with plate stacking occurring in the meridional axis of the plunger. In contrast, in Fig. 5b [iii-A] the material appears less organised and becomes more granular in appearance towards its outermost margin. Fig. 5c and d draw attention to the continuum of pine-tree like structures throughout the side walls of the plunger. The platy structure observed in Fig. 5b [iii-B] is magnified and drawn schematically in Fig. 6 The schematic of the central plunger in Fig. 6 is based on the SEM micrograph of a plunger fractured parallel to the meridional axis, as shown in Figs. 4a and

5a. Fig. 6 highlights three important regions of the plunger: (a) the interface between the outermost layer and the middle pine-tree-structured layer, (b) the layered sandwich composite structure, and (c) the plate-like arrays in the side walls. The microstructure of the plunger is significantly different from that of adjacent parts of the chela where such specialised architectures are not seen. SEM examples are provided in Fig. 7a and b showing cross-sections of the dactyl tip and the centre of the chela propodus (cf. Fig. 1). Both these parts are essentially adjacent to the dactyl plunger, the dactyl tip being representative of the anterior chela and the chela propodus representing chela shell material posterior to the dactyl plunger. In Fig. 7a, the dactyl tip is seen to comprise a solid layer cross-section without any porous centre, while in Fig. 7b, the chela propodus is a striated structure lacking the thick porous central layer that is observed in the dactyl plunger.

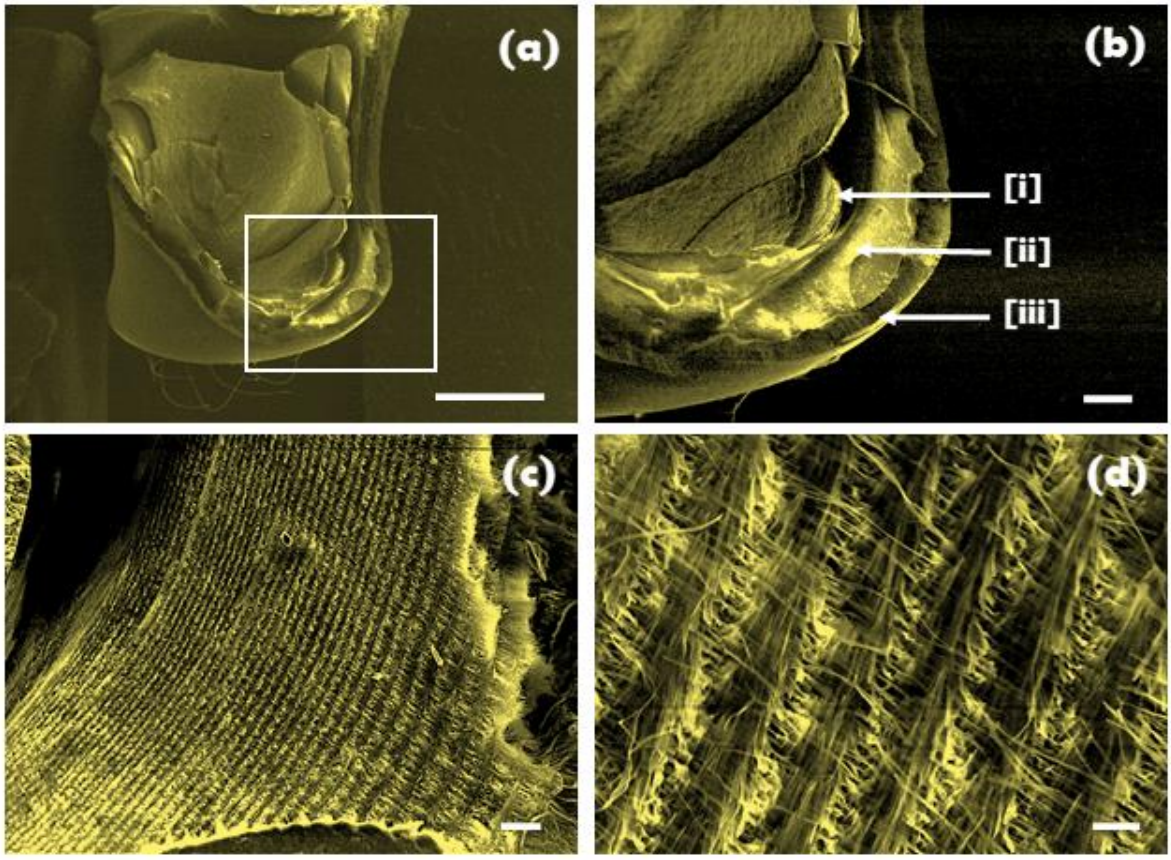

Fig. 4. SEM micrographs of (a) the cross-section of a fractured plunger (scale bar = 1 mm), (b) the bottom of the fractured plunger identifying the inner [i], middle [ii] and outer [iii] layers (scale bar = 200 μm), (c) a closer view of the middle layer showing it to be a laminated porous structure comprising pine-tree-shaped matter (scale bar = 20 μm), and (d) a higher magnification of the porous pine-tree structures (scale bar = 3 μm).

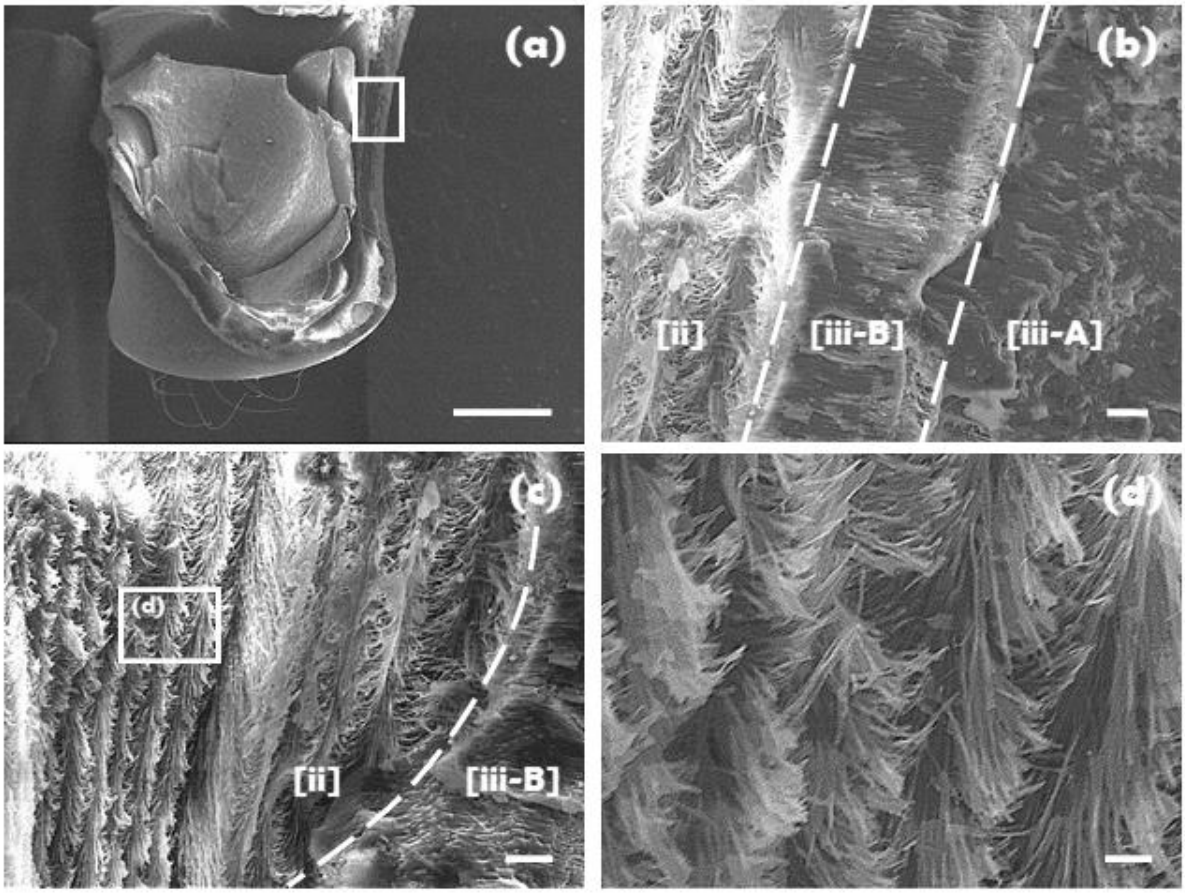

Fig. 5. SEM micrographs of (a) the cross-section of a fractured plunger (scale bar = 1 mm), (b) a closer view of the side of the fractured plunger (magnification of the box in (a)) identifying the porous middle layer composed of pine-tree-shaped matter in [ii], a plate-like inner lamina of the outer layer in [iii-B] and a more granular outer lamina of the outer layer in [iii-A] (scale bar = 10 μm), (c) a closer view of the transition between the middle layer [ii] and the plate-like layer [iii-B] (scale bar = 10 μm), and (d) a higher magnification of the middle layer pine-tree structures (scale bar = 1 μm).

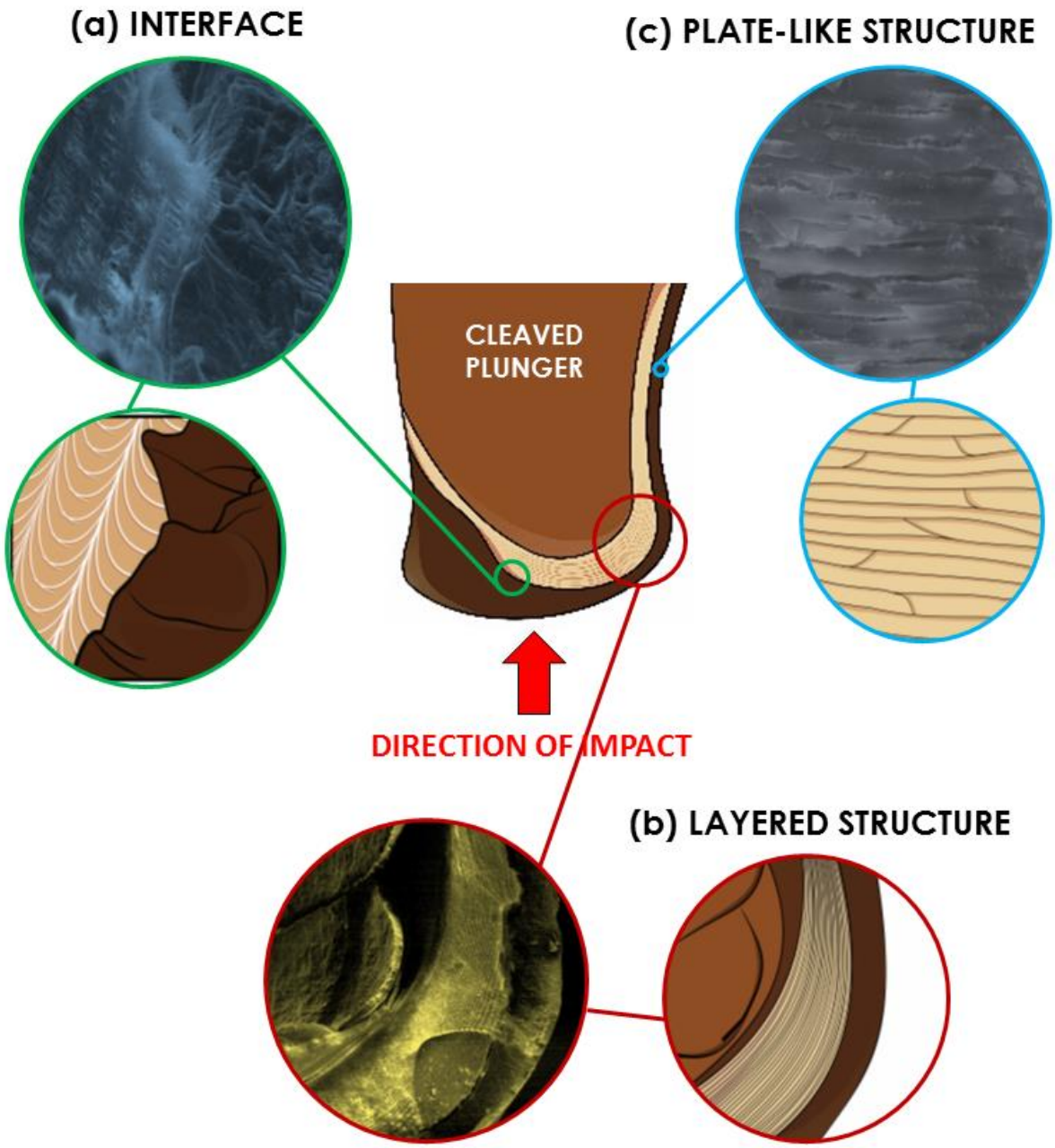

Fig. 6. Illustrative schematic of the SEM images focusing on (a) the interface between the outer and middle layers, (b) the triple layer structure of the plunger, and (c) plate-like structures forming the inner section of the outer layer in the side walls of the plunger.

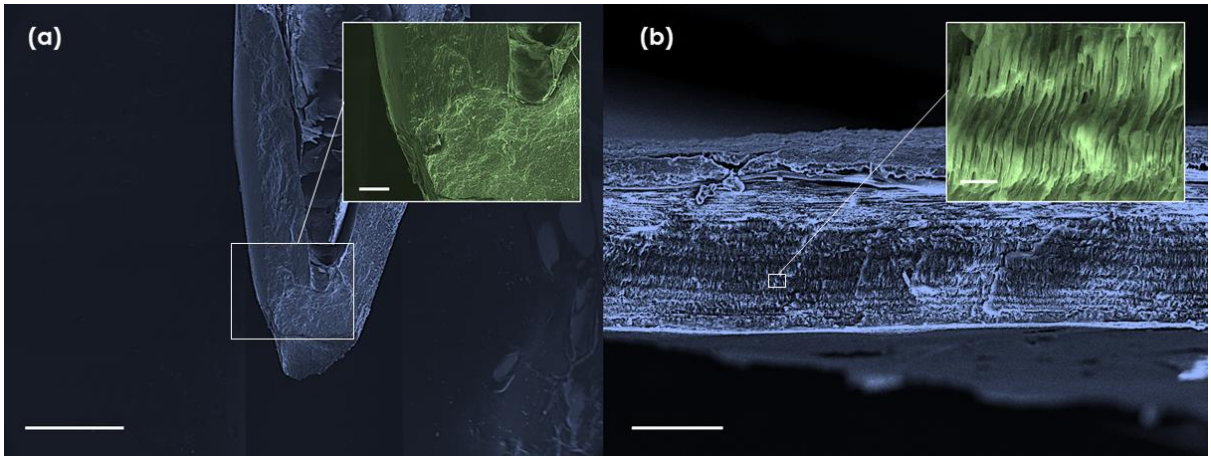

Fig. 7 SEM images of (a) the dactyl tip showing a compact structure devoid of porosity or any laminated arrangement as observed in the dactyl plunger (scale bar = 1 mm, scale bar inset = 100 μm); (b) the chela propodus exhibits a striated structure and is devoid of the high-porosity laminated arrangement observed in the dactyl plunger (scale bar = 100 μm, scale bar inset = 5 μm).

3.3. Chemical characterisation of the plunger and its cross-section

FTIR spectroscopic results from the snapping shrimp plunger (Fig. 8a) reveal the presence of β-chitin through identification of the amide I peak at 1650 cm^{-1} as well as an amide II shoulder at 1040 cm^{-1} (Sanka et al., 2016). -CH2 peaks at 2893 cm^{-1}, 2931 cm^{-1} and 2977 cm^{-1} are typical vibration frequencies arising through the presence of chitin (Cardenas et al., 2004). A small amide III shoulder peak is noticeable at 970 cm^{-1}, and this is a characteristic peak for chitin (Sanka et al., 2016). The peaks at 1040 cm^{-1} and 1070 cm^{-1} reveal the hexose-based carbohydrate backbone of chitin (Furuhashi et al., 2009). Since the α-chitin double peak is absent from the spectrum (secondary peak at 1660 cm^{-1}), we posit that β-chitin predominates (Jang et al., 2004). The reasoning for this position is that β-chitin crystals are laden with internal hydrogen bonds that effectively hold the crystal structure together. These bonds derive from interactions between the amide I (-C=O) and the amide II (-NH-) carbonyl groups, giving rise to a specific single peak at 1650 cm^{-1}. The presence of hydrogen bonding is further substantiated by the (-N-H-) vibrational peak at 1404 cm^{-1}, which occurs through hydrogen bonding with amine groups (Prabu and Natarajan, 2012). As is common in biogenic calcite, a calcite peak would be visible at 710 cm^{-1}; however, in the FTIR spectrum of Fig. 8a we find this peak has shifted to 715 cm^{-1} as a shoulder, indicating the substitution of magnesium ions into the biogenic calcite (Feilini et al., 1998). Magnesium presence in calcium carbonate is a well-documented phenomenon; it is most commonly found in the calcite form of calcium carbonate (Becker et al., 2005) and may be involved in contributing to calcium carbonate stabilisation (Raz et al., 2003; Politi et al., 2010). Alongside a shoulder peak at 1442 cm^{-1} and a specific peak at 874 cm^{-1} (visible in Fig. 8a), the calcite polymorph of calcium carbonate normally exhibits only one extra shoulder peak at either 710 cm^{-1} (for pure calcite) or 715 cm^{-1} for magnesium calcite. The aragonite polymorph of calcium carbonate can be identified alongside the calcite peaks; aragonite exhibits an extra shoulder peak at 696 cm^{-1}, which is noted in our spectrum. Given the information from the FTIR

spectrum, we assume that the primary materials present in the snapping shrimp plunger are chitin (predominantly β-chitin), magnesium calcite, and aragonite.

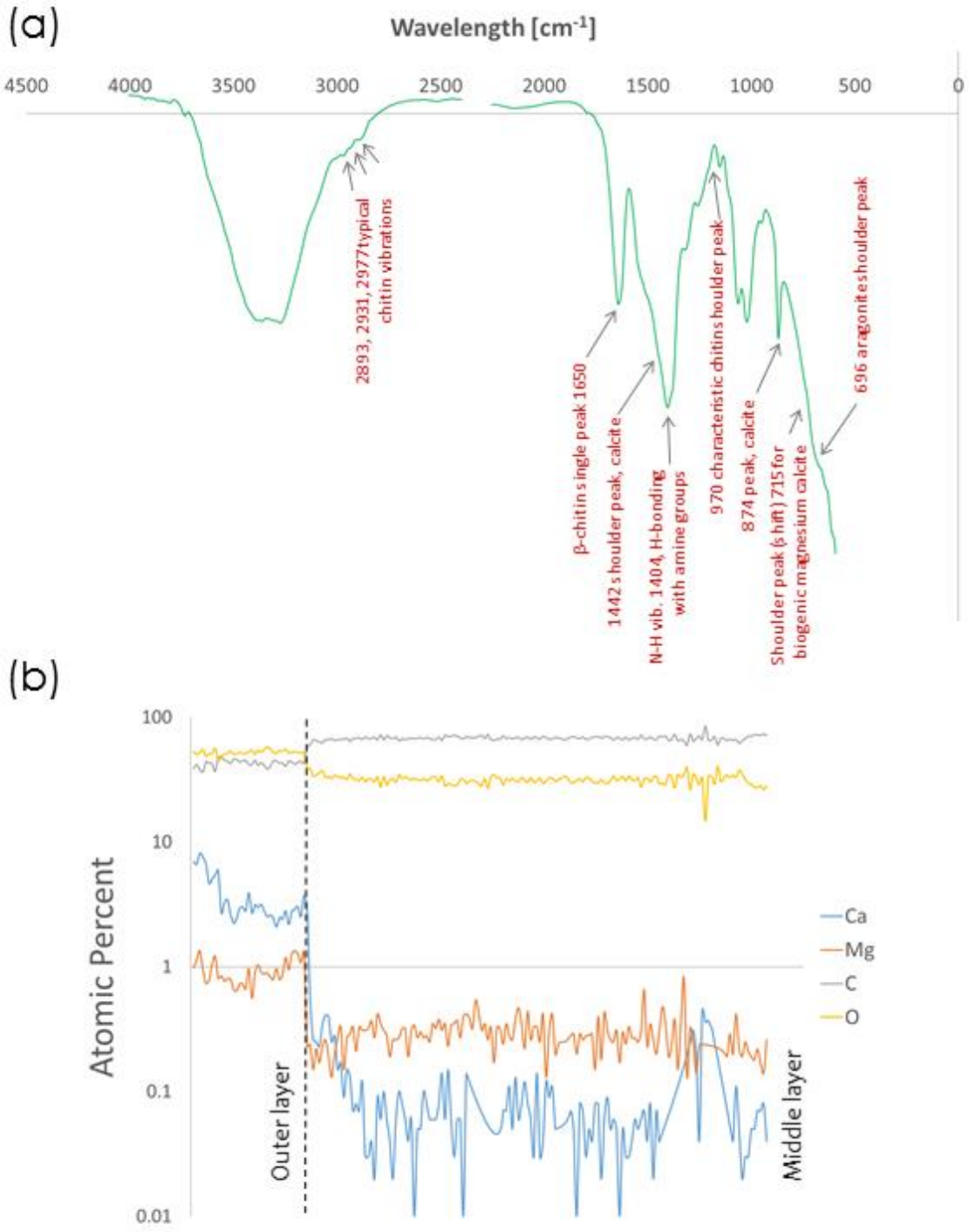

Fig. 8. (a) FTIR spectrum of the plunger and (b) EDS line scan across the outer/middle layer interfaces.

A simple means to discriminate the calcium carbonate-richer regions of the plunger from the chitin-richer regions is by energy dispersive X-ray spectroscopy (EDS). Fig. 8b shows an EDS

line scan across the interface between the outer layer and the middle layer (cf. Fig. 4b). EDS maps of the specific interface scanned for Fig. 8b are provided in Fig. 9. When examining both Fig. 8b and Fig. 9, it seems apparent that whereas the outer layer of the plunger is predominantly magnesium-substituted calcium carbonate, the middle layer material contains almost no metal atoms (< 0.1% Ca and < 1% Mg), indicating that the middle layer is composed almost solely of chitin.

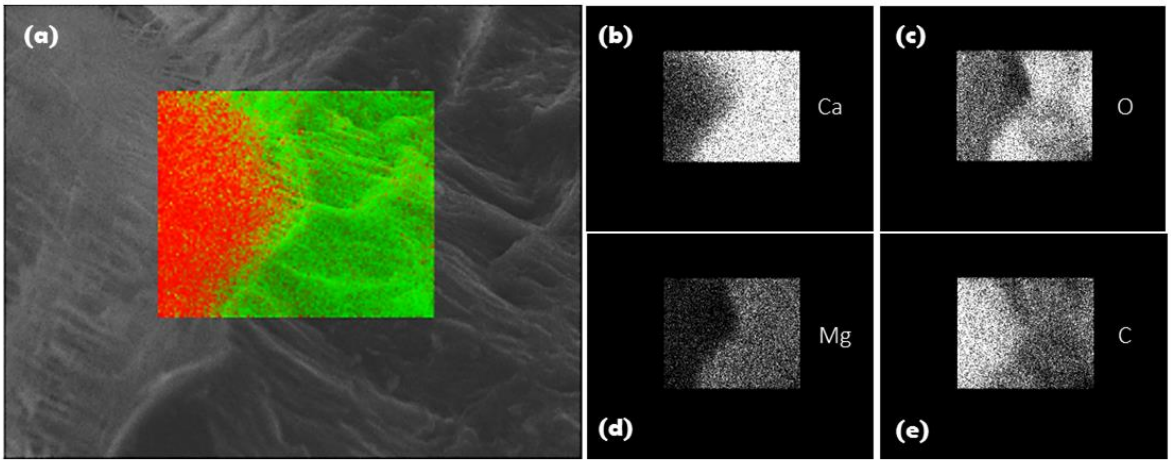

Fig. 9. EDS maps across the outer/middle layer interfaces showing (a) Ca in green and C in red, (b) Ca, (c) O, (d) Mg, and (e) C.

3.4. Heat and stress transfer modelling through the thickness of the plunger

Fig. 10a shows the heat transfer through the plunger cross-section by means of a surface plot. The purpose of this model is to determine the expected pattern of heat transfer from layer to layer as a function of pressurisation times ranging between 1 and 5 ms (Schein, 1975) (Fig. 10b). We note that at each hold-time, the temperature decreases rapidly as the heat enters the middle porous chitin-rich layer. As the pressurisation time is increased, so too does the level of heat at the surface of the plunger and the distance it travels through the plunger before it reaches a final temperature of 30 °C. The heat transfer pattern observed in this model follows a trend that is expected of sandwich composites comprising materials with different thermal conductivities (Mullholland and Cobble, 1972; Onyejekwe, 2002). A build-up of heat at the interfaces between layers is also noticeable, a phenomenon reported by Nakayama (2003) as occurring between composite interfaces due to changes in the material properties disrupting flux.

During capture, we observed that in extreme cases snapping shrimps snap rapidly and in succession when threatened. The frequency of snapping tends to decrease dramatically as a function of increasing time. We simulated an extreme 'under threat' scenario with a consecutive sequence of three 1 ms snaps with the aim of discerning the effect on heat transfer through the plunger. Fig. 10c shows a similar temperature evolution pattern to those seen in Fig. 10b, except that for each successive snap, the rate of increase in surface heat and penetration is exponential. Since there is little time for heat dissipation and convection out of the material between successive snaps, the temperature through the

plunger cross-section increases with each snap. A reduction in the rate at which heat evolves is noticeable as the heat enters the chitin-rich middle layer. The slowing down of heat transfer is a means of heat retention (insulation) and this may be present as a means to improve thermal damage tolerance.

From a mechanical perspective, the plunger experiences the highest stresses in the outer and inner layers (Fig. 10d), with the highest stresses found in areas localised in the corners. Though corners are well known to be stress concentrators, it should be noted that the radius of curvature in the modelled structure is tighter than in the actual plunger and the magnitude of stress concentration in the real plunger is expected to be less acute than shown in the model. The middle layer experiences more strains than the outer and inner layers (Fig. 10e) and perhaps relieves the plunger of concentrated mechanical energies that might otherwise lead to fracture. Plunger corners experience the highest stresses and strains.

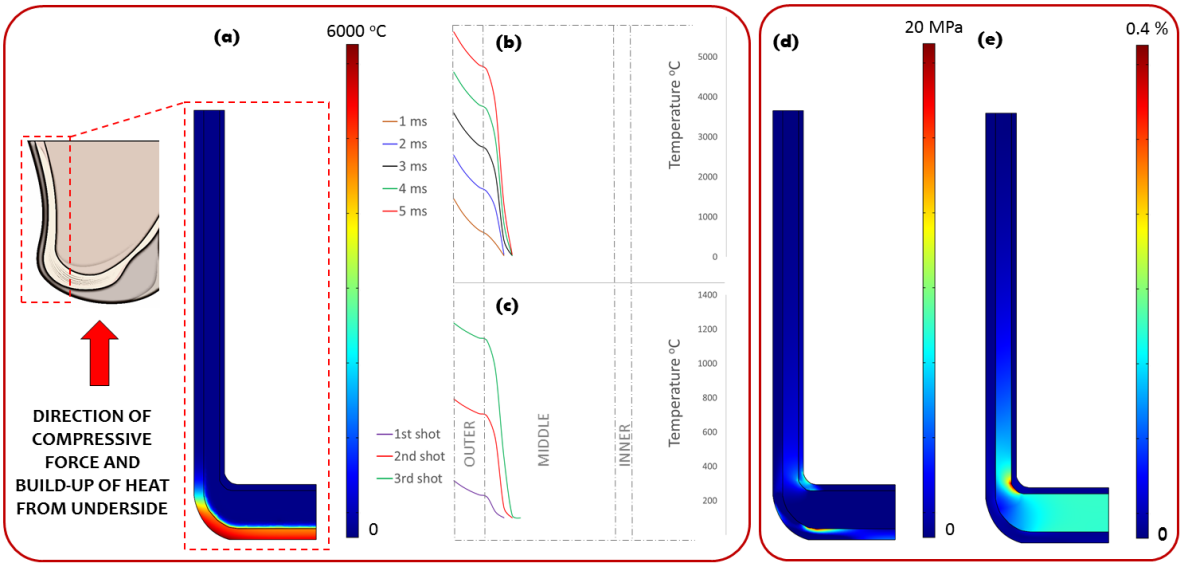

Fig. 10. Surface plot showing (a) the temperature distribution from the bottom of the plunger after a 5 ms hold, (b) the heat transfer through the bottom of the plunger at different millisecond hold times with a starting temperature of 6000 °C, (c) the heat transfer through the bottom of the plunger after 3 successive 1 ms holds with a starting temperature of 2500 °C, (d) the axial stress distribution during compression of the base of the plunger, and (e) the axial strain distribution during compression of the base of the plunger.

4. Discussion

4.1. Snapping forces

Marine decapod exoskeletons have presumably evolved as a means of protection and thus exhibit designs that withstand mechanical forces. This has been especially evident in reports on dactyl chelae and the forces they are able to withstand. Of the different marine decapod exoskeletal parts, the chelae tend to have superior mechanical properties (Dutil et al., 2000), sometimes far exceeding the properties of the carapace or merus. The chela tip is the most

heavily calcified region and exhibits a higher stiffness and fracture resistance than the rest of the chela (Tsunenari and Oya, 2016). In the snapping shrimp, the plunger–socket system is essentially a modified dactyl chela (Toth and Bauer, 2008), the 'tips' being analogous with the plunger and socket. As such it might be fair to assume that snapping forces should be at least similar to, if not higher than, typical chela closing forces of other marine decapods of similar size (Levinton and Judge, 1993; Dutil et al., 2000). Both chela shape and style also play crucial roles in the magnitude of force experienced by the chela on closing (Claverie and Smith, 2007) and the modified plunger–socket chela tips of the snapping shrimp, having the design of a high-pressure vessel, will more than likely generate greater stress within the chela system as pressure builds up through snapping, adding to the force of closure. Chela closing forces are commonly reported in the literature, ranging between ca. 10 and 250 N over a variety of different decapod species (Elner and Campbell, 1981; Block and Rebach, 1998). These values tally somewhat with the ca. 200–500 N strike forces of mantis shrimps, as reported by Patek and Caldwell (2005). Pressure within the plunger–socket system of a snapping shrimp is a potential source of mechanical damage. Recognising that the diameter of the plunger in our surveyed shrimps was never greater than ca. 2 mm, the minimum stress, excluding pressure, at the bottom of the plunger under snapping forces of 10–250 N may range from 3 to 80 MPa. Including the effect of pressurisation through plunger–socket closure, we would expect this value of stress to increase further and it would thence be logical that mechanical damage tolerance is accounted for in the dactyl plunger. Reports on the expected failure stresses of marine decapod exoskeletons range from 10 to 120 MPa (Palmer et al., 1999; Chen et al., 2008; Tsunenari and Oya, 2016).

3.2. Mechanical damage tolerance of the plunger

Here we posit that the thick mineral outer layer contributes to mechanical damage tolerance, since mechanical properties are known to increase as a function of increased calcification (Verma and Tomar, 2015). The double bilayer structure of the outer mineral-rich layer (cf. Fig. 5b) is presumably composed of ordered aragonite (Fig. 6c) where we see striated bands of mineral, and of (less ordered) magnesium calcium carbonate on the outside. Similar bilayer structures of aragonite and calcite are reported to occur in certain marine gastropods such as the abalone shell *Haliotis* (Dauphin et al., 2014), and the aragonitic layers are typically plate-like in organisation with soft interfaces, and are able to absorb considerable mechanical energy (Lin and Meyers, 2005). We suggest that the stacking of aragonite plates perpendicularly to the meridional direction, where the scalar of force is expected to be highest during snapping, is a design that improves damage tolerance in the side walls. Such aragonite plates may also resist buckling forces, which might otherwise be a problem in the side walls since they are geometrically long and thin, and thus have reduced stability under loading.

Magnesium calcium carbonate, which is predominant within the outer layer of the plunger, is also a hard and stiff material, and it is understood that the substitution of magnesium for calcium into the carbonate does not detrimentally affect either stiffness or hardness (DeVries et al., 2016). In mantis shrimp (*Odontodactylus scyllarus*) dactyl clubs, where the need to resist high impact forces is critical, stiffness and hardness values can exceed 60 GPa and 3.5 GPa,

respectively (Weaver et al., 2012). Yet, the values of the exoskeletons of shallow water shrimps are not significantly lower, with ca. 30 GPa and 1.5 GPa reported for stiffness and hardness, respectively (Verma and Tomar, 2014), especially considering that the need for protection is not as pressing as in the case of the mantis shrimp dactyl club. Crab (*Cancer magister*) chelae that are slightly more calcified than shrimp exoskeletons are reported to have stiffness and hardness values as high as 55 GPa and 2.5 GPa, respectively (Lian and Wang, 2014). These values are not far lower than those reported for mantis shrimp dactyl clubs (Weaver et al., 2012) and as such we deduce that chela tips that are highly calcified tend to be equally stiff and hard, with only slight variations arising due to ecological, environmental or behavioural factors. Since the dactyl plunger (chela) of the snapping shrimps researched herein has heavily calcified outer layers, we reason that its stiffness and hardness are likely to be in a similar range as those reported of *C. magister* (Lian and Wang, 2014) and *O. scyllarus* (Weaver et al., 2012). Here, we note that the plunger corners experience the highest stresses and strains, and we postulate that while the stiff outer and inner layers resist load, the middle layer strains more and is able to dissipate mechanical energy more effectively. Chitin strain is increased by its high porosity, and this may be of further benefit in dissipating mechanical energy.

Damage tolerance against high pressures exerted upon the dactyl plunger will also arise from the presence of a chitin–mineral interface (Qu et al., 2015). In their paper, Qu and co-workers conclude that organic–inorganic interfaces between chitin and calcite improve the toughness of biomaterial systems through a combinatorial effect of viscous interfaces and interfacial shearing that encourages viscoelastic behaviour and mechanical energy dissipation at the interfaces. Such interfaces, as observed within the snapping shrimp dactyl plunger, will likely have similar characteristics; however, the large percentage of free volume between the chitin pine-trees would additionally permit significant deformation of the pine-trees prior to a more viscous style of shear deformation at the organic–inorganic interface.

3.3. Thermal damage tolerance of the plunger

The organisation of the snapping shrimp dactyl plunger, as revealed above, exhibits a sandwich composite architecture that bears a very mild similarity to the bi-layer composite arrangement of the mantis shrimp dactyl club (Guarin-Zapta et al., 2015), which itself comprises a thick, hard mineral shell, underneath of which is a softer chitin-rich region. A most obvious difference between the two, however, is noticeable in the arrangement and architecture of the chitin-rich regions. The dactyl club of the mantis shrimp exhibits a dense, helicoidally arranged chitin-rich (Bouligand) region with little, if any, porosit. In contrast, in the snapping shrimp, the chitin-rich region is extremely porous and the chitin grows into pine-tree like structures, arranged into a quasi-laminated construct, which presumably has a function in, at least, retarding heat flux. It is interesting to note that we do not see clear evidence of a Bouligand arrangement in the chitin-rich region of the plunger, though it is possible that if Bouligand structures were made porous, they would look like connected and layered pine-trees, as elucidated herein. The porosity of the chitin-rich layer of the *Alpheus* sp. dactyl plunger is on average 0.46 (standard deviation ± 0.096), which is almost half the

entire layer volume. To the best of our knowledge, this is the first time that porous pine-tree-like chitin has been observed in any marine animal. Since there are no reports on heat transfer through marine decapod chelae, dactyls or exocuticles, we modelled heat transfer through the sandwich composite layout of the bottom of the snapping shrimp dactyl plunger. Our model results reveal that the chitin-rich layer has a benefit in that it can insulate interior parts of the plunger, and perhaps any underlying soft tissues, from heat that evolves as a function of plunger–socket snapping pressures. If high temperatures reach the inner regions of the plunger, this may detrimentally affect essential biological functions for snapping shrimps or, in the worst case, may cause permanent, irrecoverable heat damage to cells and proteins. To this effect, the broader chitin laminae, situated closer to the outer layer (cf. Fig. 4) have an additional benefit in that they are more porous than the inner laminae and will be more effective in insulating inner materials from heat, though this particular thermostructural aspect is not reflected in our model. Importantly, heat evolution from shorter held (and pressurised) snaps does not tend to dissipate through the cross-section as far as longer held (and pressurised) snaps. Heat does build up, nevertheless, and consecutive snaps promote the evolution of heat through the plunger cross-section, a situation that might arise, for example, when the shrimp is threatened. In our model, we used closure times of 1–5 ms, which are snap closure times reported for the species *Alpheus heterochaelis* (Schein, 1975) and the difference between the outermost temperature and that in the inner layer is approximately 500%. Heat drops through the outer layer of the plunger but then falls at a considerable rate as soon as it contacts the insulating middle layer. We also modelled three successive snaps based on both our own observations of the (initial stage) continual snapping behaviour of shrimps when under threat and claw closure times of fiddler crabs reported by Levinton et al. (1995), who recorded up to two rapid claw closures per second and up to a total of 10 closures within an 8 second range when these crabs are attacking prey. We find that heat builds up exponentially when snapping is successive, which is potentially more damaging to the materials of the plunger. There is certainly some degree of variability between the species and the conditions under which decapods rapidly close their chelae; however, in the case of snapping shrimps, the heat generated within the plunger–socket system is so high that lengthy plunger–socket closures may be thermally damaging to the materials. High temperature exposure can decompose chitin and degrade the properties of minerals such as biogenic calcite (Verma and Tomar, 2015), which is perhaps why snapping shrimps employ a 'cocking delay' of approximately 500 ms between successive snaps (Herberholz and Schmitz, 1998). From a behavioural viewpoint, shrimps will often retreat after snapping (Herberholz and Schmitz, 1998), which may further act as a delay between successive snaps, thus allowing heat caught up within the plunger to convect prior to a consecutive snap. Delay between snaps is especially important if indeed snaps are in succession, and more so if the snap closure time is lengthened (Stein, 1975). Thermomechanical damage tolerance is vital to snapping shrimps since heat damage to the shrimps' exoskeletal matter may result in reduced properties (Verma and Tomar, 2015) or fracture. Conover and Miller (1978) reported that once snapping shrimp dactyls fracture, the shrimps lose their ability to snap. An inability to snap, and hence release a high pressure

cavitation bubble, would render the shrimp vulnerable to attack, and would reduce its predatory and mating success (Schein, 1975).

5. Conclusions

In conclusion, we found that *Alpheus* shrimp have highly organised dactyl plungers, with a sandwich composite arrangement. Following both chemical and optical characterisation, we conclude that the plunger is a tri-layer structure at the millimetre length scale. The outermost and innermost layers consist of biogenic minerals including aragonite and magnesium calcite, while the middle layer is chitin-rich, with close to 50% porosity. By modelling heat transfer, we found that heat advances through the dactyl plunger cross-section through successive snaps, and that the middle layer insulates against heat. Since the outer and inner layers are made of biogenic mineral-based materials, with a clear level of organisation in areas where forces might cause damage, we also suggest that the dactyl plunger has the coupled characteristics of thermal and mechanical damage tolerance.

Acknowledgements

We thank the following individuals for their gracious help in specimen collection: Kresty Ani Yani, Abdullah Firaswan, Dalton Surya Prayoga, Rida Nurafiati, Emma Permata Hati, Matin Nuhamunada, Made Sania Saraswati, KSK-Crustacea5 Group. We thank the Cell Fate Laboratory at the Turku Centre for Biotechnology for allowing us to use their laboratory.

Appendix A. Supplementary data

Supplementary data associated with this article can be found in the online version at doi: ###.

References

Anker A, Ahyong ST, Noël PY, Palmer AR, 2006. Morphological phylogeny of alpheid shrimps: parallel preadaptation and the origin of a key morphological innovation, the snapping claw. Evolution 60, 2507–2528.

Au WWL, Banks K, 1997. The acoustics of the snapping shrimp *Synalpheus parneomeris* in Kaneohe Bay. J. Acoust. Soc. Am. 103, 41-47.

Becker A, Ziegler A, Epple M, 2005. The mineral phase in the cuticles of two species of Crustacea consists of magnesium calcite, amorphous calcium carbonate, and amorphous calcium phosphate. Dalton Trans. 21, 1814-1820.

Block D, Rebach S, 1998. Correlates of claw length in the rock crab, *Cancer irroratus* (Decapoda, Brachyura). Crustaceana 71, 468-473.

Boltana S, Thiel M, 2001. Associations between two species of snapping shrimp, *Alpheus inca* and *Alpheopsis chilensis* (Decapoda: Caridea: Alphidae). J. Mar. Biol. Ass. UK 81, 633-638.

Boomsma K, Poulikakos D, 2001. On the effective thermal conductivity of a three-dimensional fluid-saturated metal foam. Int. J. Heat Mass Transfer 44, 827-836.

Buonanno G, Carotenuto A, 2000. The effective thermal conductivity of packed beds of spheres for a finite area. Num. Heat Transfer A 37, 343-357.

Caldwell RL, 1991. Variation in reproductive behaviour in stomatopod crustaceans. In: Bauer RT, Martin JW (Eds.), Crustacean Sexual Biology. Columbia University Press, New York, pp. 67-90.

Cardenas G, Cabrera G, Taboada E, Miranda SP, 2004. Chitin characterisation by SEM, FTIR, XRD and 13C cross polarisation/mass angle spinning NMR. J. Appl. Polymer Sci. 93, 1876-1885.

Chen PY, Lin AYM, McKittrick J, Meyers MA, 2008. Structure and mechanical properties of crab exoskeletons. Acta Biomat. 4, 587-596.

Chitre M, Beng KT, Potter J, 2003. Origins of directionality in snapping shrimp sounds and its potential applications. OCEANS 2003, IEEE Proceedings, San Diego.

Clauser C, Huenges E, 1995. Thermal conductivity of rocks and minerals. In: Ahrens, J (Ed.), Rock Physics and Phase Relations: A Handbook of Physical Constants. American Geophysical Union, Washington, DC, pp. 105-126.

Claverie T, Smith IP, 2007. Functional significance of an unusual chela dimorphism in a marine decapod: specialisation as a weapon? Proc. R. Soc. B 274, 3033-3038.

Conover, M.R., Miller D.E., 1978. The importance of the large chela in the territorial and pairing behavior of the snapping shrimp, *Alpheus heterochaelis*. Mar. Behav. Physiol. 5, 185-192.

Dauphin Y, Cuif JP, Castillo-Michel H, Chevallard C, Farre B, Meibom A, 2014. Unusual micrometric calcite–aragonite interface in the abalone shell *Haliotis* (Mollusca, Gastropoda). Microsc. Microanal. 20, 276-284.

DeVries MS, Webb SJ, Tu J, Cory E, Morgan V, Sah RL, Deheyn DD, Taylor JRA, 2016. Stress physiology and weapon integrity of intertidal mantis shrimp under future ocean conditions. Sci. Rep. 6, 38637.

Downer, J. 2002. Weird Nature: An Astonishing Exploration of Nature's Strangest Behavior. Firefly Books, Ontario.

Dutil JD; Rollet C, Bouchard R, Claxton WT, 2000. Shell strength and carapace size in non-adult and adult male snow crab (*Chionoecetes opilo*). J. Crust. Biol. 20, 399-406.

Edgar, R.C., 2004. MUSCLE: a multiple sequence alignment method with reduced time and space complexity. BMC Bioinf. 5, 113.

Elner RW, Campbell A, 1981. Force, function and mechanical advantage in the chelae of the American lobster *Homarus americanus* (Decapoda: Crustacea), J. Zool. 193, 269-286.

Everest FA, Young RW, Johnson MW, 1948. Acoustical characteristics of noise produced by snapping shrimp. J. Acoust. Soc. Am. 20, 137-142.

Felini G, Fermani S, Gazzano M, Ripamonti A, 1998. Structure and morphology of synthetic magnesium calcite. J. Mater. Chem. 8, 1061-1065.

Fergusson BG, Cleary JL, 2001. In situ source level and source position estimates of biological transient signals produced by snapping shrimp in an underwater environment. J. Acoust. Soc. Am. 109, 3031-3037.

Folmer, O., Black, M., Hoeh, W., Lutz, R., Vrijenhoek, R., 1994. DNA primers for amplification of mitochondrial cytochrome c oxidase subunit I from diverse metazoan invertebrates. Mol. Mar. Biol. Biotechnol. 3, 294-299.

Furuhashi T, Schwarzinger C, Miksik I, Smrz M, Beran A, 2009. Molluscan shell evolution with review of shell calcification hypothesis. Comp. Biochem. Physiol. B: Biochem. Mol. Biol. 154, 351-371.

Guarin-Zapta N, Gomez J, Yaraghi N, Kisailus D, Zavattieri PD, 2015. Shear wave filtering in naturally-occurring Bouligand structures. Acta Biomat. 23, 11-20.

Herberholz J, Schmitz B, 1998. Role of mechanosensory stimuli in intraspecific agonistic encounters of the snapping shrimp (*Alpheus heterochaelis*). Biol. Bull. 195, 156–167.

Herberholz J, Schmitz B, 1999. Flow visualisation and high speed video analysis of water jets in the snapping shrimp (*Alpheus heterochaelis*). J. Comp. Physiol. A 185, 41–49.

Hess D, Brucker C, Hegner F, Balmert A, Bleckmann H, 2013. Vortex formation with a snapping shrimp claw. PLoS ONE 8, e77120.

Holthuis LB, 1980. FAO Species Catalogue. Vol. 1: Shrimps and Prawns of the World. An Annotated Catalogue of Species of Interest to Fisheries. FAO, Rome.

Hultgren, K.M., Stachowicz, J.J., 2008. Molecular phylogeny of the brachyuran crab superfamily Majoidea indicates close congruence with trees based on larval morphology. Mol. Phylogen. Evol. 48, 986–996.

Jacobs GK, Kerrick DL, Krupka KM, 1981. The high-temperature heat capacity of natural calcite ($CaCO_3$). Phys. Chem. Miner. 7, 55-59.

Jang MK, Kong BG, Jeong YII, Lee CH, Nah JW, 2004. Physicochemical characterisation of α-chitin, β-chitin and γ-chitin separated from natural resources. J. Polym. Sci. A: Pol. Chem. 42, 3423-3432.

Johnson MW, Everest FA, Young RW, 1947. The role of snapping shrimp (*Crangon* and *Synalpheus*) in the production of underwater noise in the sea. Biol. Bull. 93, 122-138.

Kim BN, Hahn J, Choi BK, Kim BC, 2010. Snapping shrimp sound measured under laboratory conditions. Jap. J. Appl. Phys. 49, 07HG04.

Kim W, Abele LG, 1988. The Snapping Shrimp Genus *Alpheus* from the Eastern Pacific (Decapoda, Caridea, Alpheidae). Smiths. Contrib. Zool. 454, 1-119.

Legg MW, Duncan AJ, Zaknich A, Greening MV, 2007. Analysis of impulsive biological noise due to snapping shrimp as a point process in time. OCEANS 2007, IEEE Proceedings, Aberdeen.

Levinton JS, Judge ML, 1993. The relationship of closing force to body size for the major claw of *Uca pugnax* (Decapoda: Ocypodidae). Funct. Ecol. 7, 339-345.

Levinton JS, Judge ML, Kurdziel JP, 1995. Functional differences between the major and minor claws of fiddler crabs (*Uca,* family Ocypodidae, order Decapoda, subphylum Crustacea): a result of selection or developmental constraint? J. Exp. Mar. Biol. Ecol. 193, 147-160.

Lian J, Wang J, 2014. Microstructure and mechanical isotropy of crab *Cancer magister* exoskeletons. Exp. Mech. 54, 229-239.

Lin A, Meyers MA, 2005. Growth and structure in abalone shells. Mat. Sci. Eng. A, 390, 27-41.

Lohse D, Schmitz B, Versluis M, 2001. Snapping shrimp make flashing bubbles. Nature 413, 477-478.

McNamara III WB, Didenko YT, Suslick KS, 1999. Sonoluminescence temperatures during multi-bubble cavitation. Nature 401, 772-775.

Mellon D, 1981. Nerves and the transformation of claw type in snapping shrimps. Trends Neurosci. 4, 245-248.

Mellon D, Stephens PJ, 1979. The motor organisation of claw closer muscles in snapping shrimp. J. Comp. Physiol. A 132, 109-115.

Mohl B, Wahlberg M, Madsen PT, Heerfordt A, Lund A, 2003. The monopulsed nature of sperm whale clicks. J. Acoust. Soc. Am. 114, 1143-1154.

Mullholland GP, Cobble MH, 1972. Diffusion through composite media. Int. J. Heat Mass Transfer 15, 147-160.

Muzzarelli RAA, 1977. Chitin. Pergamon Press, Oxford.

Nakayama W, 2003. A methodology to work on geometrically complex heat transfer systems: the cases of heat conduction through composite slabs. Int. J. Heat Mass Transfer 46, 3397-3409.

Onyejekwe OO, 2002. Heat conduction in composite media: a boundary integral approach. Comput. Chem. Eng. 26, 1621-1632.

Palmer AR, Taylor GM, Barton A, 1999. Cuticle strength and the size-dependence of safety factors in cancer crab claws. Ecol. Evol. 196, 281-294.

Patek SN, Caldwell RL, 2005. Extreme impact and cavitation forces of a biological hammer: strike forces of the peacock mantic shrimp *Odontofactylus scyllarus*. J. Exp. Biol. 208, 3655-3664.

Politi Y, Catchelor DR, Zaslansky P, Chmelka BF, Weaver JC, Sagi I, Weiner S, Addadi L, 2010. Role of magnesium ion in the stabilisation of biogenic amorphous calcium carbonate: a structure–function investigation. Chem. Mater. 22, 161-166.

Prabu K, Natarajan E, 2012. Isolation and FTIR spectroscopy characterisation of chitin from local sources. Adv. Appl. Sci. Res. 3, 1870-1875.

Qu T, Verma D, Alucozai M, Tomar V, 2015. Influence of interfacial interactions on deformation mechanism and interface viscosity in α-chitin–calcite interfaces. Acta Biomat. 25, 325-338.

Rafinesque C.S., 1815. Analyse de la Nature ou Tableau de l'Univers et des Corps Organisés. Palermo.

Raz S, Hamilton PC, Wilt FH, Weiner S, Addadi L, 2003. The transient phase of amorphous calcium carbonate in sea urchin larval spicules: the involvement of proteins and magnesium ions in its formation and stabilisation. Adv. Funct. Mat. 13, 480-486.

Ritzmann RE, 1974. Mechanisms for the snapping behaviour of two alpheid shrimp, *Alpheus californiensis* and *Alpheus heterochelis*. J. Comp. Physiol. 95, 217-236.

Rocha RPA, Cruz ME, 2001. Computation of the effective conductivity of unidirectional fibrous composites with an interfacial thermal resistance. Numer. Heat Transfer A 39, 179-203.

Saitou N., Nei M., 1987. The neighbor-joining method: a new method for reconstructing phylogenetic trees. Mol. Biol. Evol. 4, 406-425.

Sanka I, Auyono EA, Rivero-Muller A, Alam P, 2016. Carapace surface architecture facilitates camouflage of the decorator crab *Tiarinia cornigera*. Acta Biomat. 41, 52-59.

Schein H, 1975. Aspects of the aggressive and sexual behaviour of *Alpheus heterochaelis* Say. Mar. Behav. Physiol. 3, 83-96.

Tamura K., Nei M., Kumar S, 2004. Prospects for inferring very large phylogenies by using the neighbor-joining method. Proc. Natl. Acad. Sci. USA 101, 11030-11035.

Tamura K., Stecher G., Peterson D., Filipski A., Kumar S., 2013. MEGA6: molecular evolutionary genetics analysis version 6.0. Mol. Biol. Evol. 30, 2725-2729.

Toth E, Bauer RT, 2008. *Synalpheus paraneptunus* (Crustacea: Decapoda: Caridea) populations with intersex gonopores: a sexual enigma among sponge dwelling snapping shrimps. Invert. Reprod. Dev. 51, 49-59.

Uryash VF, Larina VN, Kokurina NY, Bakulin AV, Kashtnov EA, Varlamov VP, 2012. Dependence of the ordering degree and thermochemical characteristics of chitin and chitosan on their biological origin. Russ. J. Phys. Chem. A 86, 1-8.

Versluis M, Schmitz B, Von der Heydt A, Lohse D, 2000. How snapping shrimps snap: through cavitation bubbles. Science 289, 2114-2117.

Vogel S, 2003. Comparative Biomechanics: Life's Physical World. Princeton University Press, Princeton.

Wang J, Carson JK, North MF, Cleland DJ, 2006. A new approach to modelling the effective thermal conductivity of heterogeneous materials. Int. J. Heat Mass Transfer 49, 3075-3083.

Warren CG, 2010. Polymer-ceramic MEMS bimorphs as thermal infrared sensors. PhD Thesis, University of California, Berkeley.

Verma D, Tomar V, 2014. Structural-nanomechanical property correlation of shallow water shrimp (*Pandalus platyceros*) exoskeleton at elevated temperature. J. Bionic Eng. 11, 360-370.

Verma D, Tomar V, 2015. An investigation into mechanical strength of exoskeleton of hydrothermal vent shrimp (*Rimicaris exoculate*) and shallow water shrimp (*Pandalus platyceros*) at elevated temperatures. Mater. Sci. Eng. C 49, 243-250.

Weaver JC, Milliron GW, Miserez A, Evans-Lutterodt K, Herrera S, Gallana I, Mershon WJ, Swanson B, Zavattieri P, DiMasi E, Kisailus D, 2012. The stomatopod dactyl club: a formidable damage-tolerant biological hammer. Science 336, 1275-1280.

SUPPLEMENTARY MATERIAL: Species Identification

The snapping shrimp dactyl plunger: a thermomechanical damage-tolerant sandwich composite

***Corresponding author:** Parvez Alam, School of Engineering, Institute for Materials and Processes, University of Edinburgh, UK. E-mail addresses: parvez.alam@ed.ac.uk and parvez.alam@abo.fi

Genetic Barcoding Results

Using results from the sequencing of isolated tissue DNA from a snapping shrimp limb, we performed BLAST to identify the sequence homology of our sample in GenBank. We picked both the highest identity sequences and some distant identity percentages to construct the phylogenetic trees. With alignment, we ascertained two dendograms from MEGA6 (Figs. S1 and S2), which represent the phylogenetic trees of the COI and 16S snapping shrimp genes, respectively.

The snapping shrimp sequences were presented as an operational taxonomic unit (OTU). The OTU provides evidence that the sequences obtained from the snapping shrimp (COI and 16S) belong to the genus *Alpheus*. In Fig. S1, we note that there are two large groups or clades. Nevertheless, the OTU shows that the sequences belong to the *Alpheus* genus. In Fig. S2 we find species diversity, with the OTU with 16S related to the genus *Alpheus* in the GenBank database. We repeated the full procedure a second time on a different shrimp limb, which confirmed our results.

We considered the chelae, or chelipeds, as important when morphologically identifying the shrimps. The cheliped within the Alpheidae family typically has a part of the dactyl that can be embedded in the pollex cavity (Anker et al., 2006). The genus *Alpheus* is part of the Alpheidae family, which comprises approximately 71 species in two genera. The only snapping shrimp genera identified thus far from this family are *Alpheus* and *Synalpheus* (Rafinesque, 1815). The shrimp genus was morphologically determined by examining the pereopod, rostrum, somites, and the telson (Holthuis, 1980). From both the genetic and morphological results, we identify the shrimp as being an *Alpheus* species.

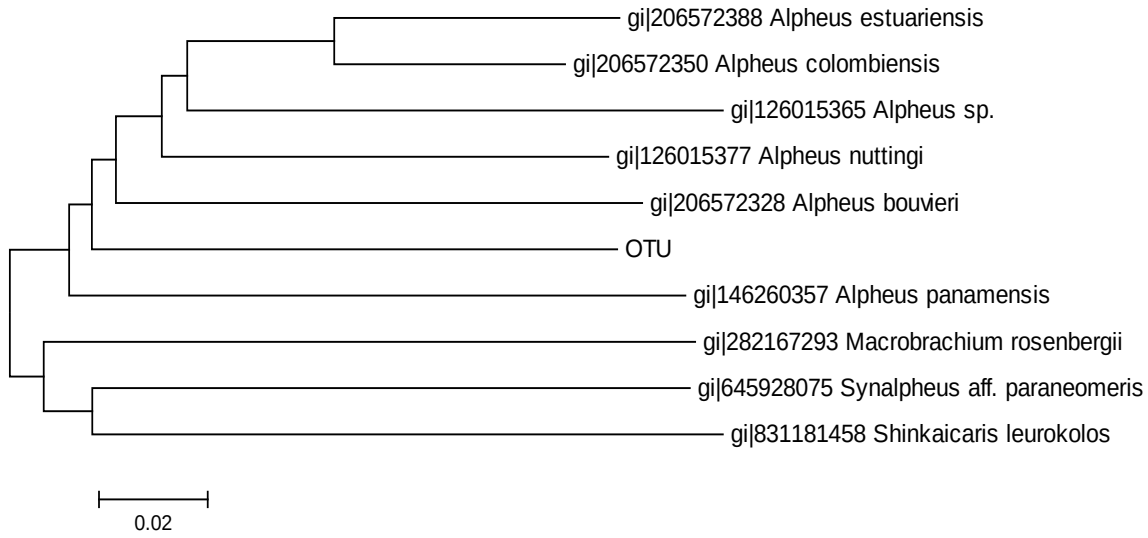

Fig. S1. Phylogenetic tree based on the COI gene sequence.

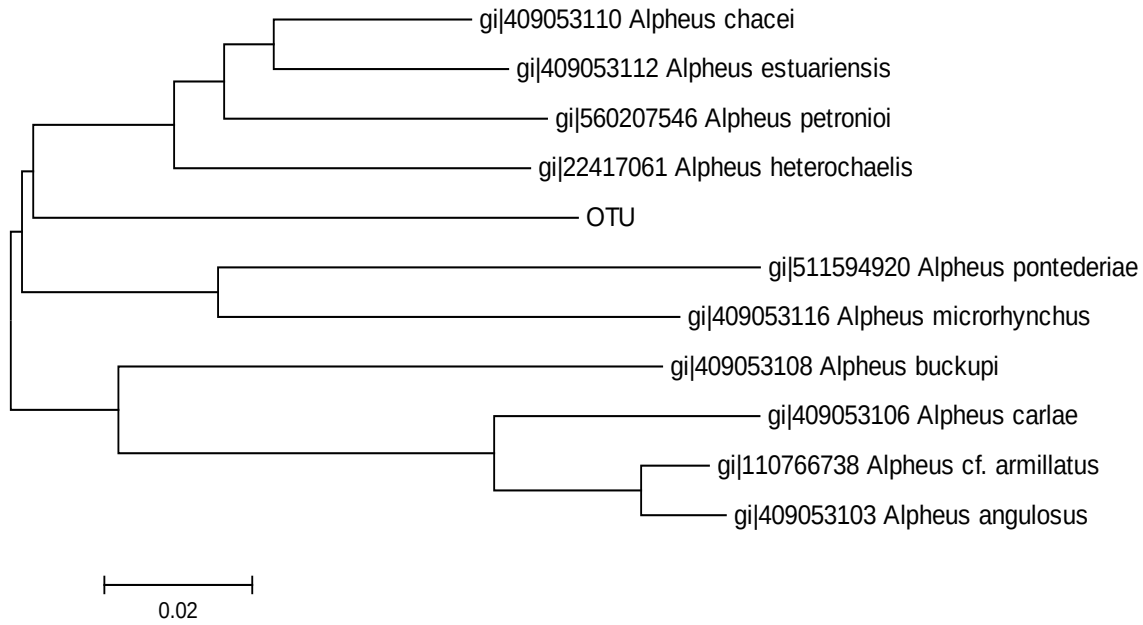

Fig. S2. Phylogenetic tree based on the 16S gene sequence**.**

References

Anker, A., Ahyong, S.T., Noël, P.Y., Palmer, A.R., 2006. Morphological phylogeny of alpheid shrimps: parallel preadaptation and the origin of a key morphological innovation, the snapping claw. Evolution Int. J. Org. Evol. 60, 2507–2528.